Nanotechnology, Science and Applications

Dovepress
Taylor & Francis Group

Open Access Full Text Article

ORIGINAL RESEARCH

An Approach to Enhance the Solubility of an Atypical Antipsychotic Drug, Aripiprazole: Design, Characterization, and Evaluation of Arabinoxylan-Based Nanoparticles

Mehwish Sikander[1], Ume Ruqia Tulain[1], Nadia Shamshad Malik[2], Arshad Mahmood[3,4], Mohammed S Alqahtani[5], Alia Erum[1], Muhammad Tariq Khan[2,6]

[1]Faculty of Pharmacy, University of Sargodha, Sargodha, Pakistan; [2]Faculty of Pharmacy, Capital University of Science and Technology, Islamabad, Pakistan; [3]College of Pharmacy, Al Ain University, Abu Dhabi Campus, Abu Dhabi, United Arab Emirates; [4]AAU Health and Biomedical Research Center (HBRC) Al Ain University, Abu Dhabi, United Arab Emirates; [5]Nanobiotechnology Unit, Department of Pharmaceutics, College of Pharmacy, King Saud University, Riyadh, Saudi Arabia; [6]Department of Pharmacy, Quaid-i-Azam University, Islamabad, Pakistan

Correspondence: Ume Ruqia Tulain, Faculty of Pharmacy, University of Sargodha, Sargodha, Pakistan, Tel +00923316668588, Email umeruqia_tulain@yahoo.com

Introduction: Natural polymers have emerged as versatile and sustainable alternatives to synthetic polymers in pharmaceutical and biomedical applications. This study focuses on the extraction of arabinoxylan (AX) from maize husk and its potential as a promising excipient to enhance the solubility and oral bioavailability of Aripiprazole (APZ), a poorly water-soluble antipsychotic drug, offering a robust strategy for overcoming challenges associated with hydrophobic drugs.

Methods: APZ-loaded AX nanoparticles were synthesized using the ionotropic gelation technique. The formulation with the highest encapsulation efficiency designated as FN4 was selected for detailed characterization. Various analytical techniques, including Scanning Electron Microscopy (SEM), X-ray Diffraction (XRD), and Differential Scanning Calorimetry (DSC), were employed to assess the morphological, crystalline, and thermal properties of the nanoparticles. In vitro release studies were conducted on both simulated gastric fluid (pH 1.2) and simulated intestinal fluid (pH 6.8) to evaluate drug dissolution behaviour. The everted sac method was utilized to assess the permeation and transport of APZ from the AX-based nanoparticles.

Results: The FN4 formulation exhibited an encapsulation efficiency of 88.9% ± 1.77%, with a particle size of 284.4 nm, a polydispersity index (PDI) of 0.346, and a zeta potential of 20.7 mV. SEM analysis revealed a uniform distribution of polyhedral-shaped nanoparticles. XRD and DSC analyses indicated that APZ was in an amorphous state within the nanoparticles. Drug release was more pronounced at pH 6.8, with the AX nanoparticles showing sustained release. The everted sac method demonstrated enhanced permeation of APZ across intestinal membranes, supporting the potential of AX nanoparticles in improving drug absorption.

Discussion: The AX-based nanoparticle formulation significantly improved the solubility, pH-dependent release profile, and sustained release of APZ, offering a promising strategy to enhance the oral bioavailability of poorly soluble drugs. These findings suggest that AX nanoparticles could serve as an effective delivery system for enhancing the therapeutic potential of hydrophobic drugs like APZ.

Keywords: arabinoxylan, aripiprazole, nanoparticles, bioavailability, solubility

Introduction

The pharmaceutical industry has shown a great deal of interest in natural polymers, or biopolymers, particularly polysaccharides, because of their high reactivity, safety, biodegradability, and biocompatibility. Moreover, they are found to be economic due to their abundance and biodiversity.[1] Natural polymers were mostly extracted from micro-organisms and plants. Arabinoxylan (AX) is a natural polysaccharide isolated from Maize (Zea mays) seed husk through the process of alkaline hydrolysis.[2] AX is hemicellulose having attached arabinose side chains to a linear backbone (β-

Received: 10 November 2024
Accepted: 29 January 2025
Published: 27 February 2025

(1→4)-linked D-xylopyranosyl units). AX has biomedical applications due to its biocompatibility, water absorption and drug delivery characteristics.[3]

Since most bioactive ingredients are poorly soluble in water, the goal of developing nanoparticles is to increase the bioavailability of the bioactive elements at a greater surface/volume ratio. In the last twenty years, research in the pharmaceutical sector has concentrated mostly on obtaining microparticles and nanoparticles of coprecipitates comprising a drug and a suitable polymeric carrier.[4] Solid particles or particle dispersions of sizes from 1 to 1000 nm are considered nanoparticles. Due to their smaller particle size, better drug dissolving rates and enriched absorption were accomplished. Furthermore, they release the drug molecules in a controlled manner.[2]

Aripiprazole (APZ) was approved by the U.S. Food and Drug Administration (FDA) in November 2002 for the therapy of schizophrenia.[5] APZ a "second generation atypical antipsychotic" has some problems associated with its oral delivery such as extensive hepatic metabolism, presence of enzymes and pH of stomach inactivating the drug. All these problems affect the absorption and bioavailability of APZ reducing its in-vivo efficacy.[6] Furthermore, APZ is a BCS Class IV drug (low solubility and permeability) having poor oral bioavailability. The best approach to improve drug bioavailability is the development of a drug delivery system by reducing the particle size to a nanometre scale. Particle size reduction increases the surface area leading to an enhanced dissolution rate. The nanoparticulate system plays a role in enhancing drug bioavailability by improving its absorption through increased solubility.[7] Nanotechnology plays a pivotal role in addressing the challenges of dissolution and permeability by modifying the physicochemical properties of drugs. This alteration often results in beneficial effects on drug bioavailability, further enhancing the efficacy of drug delivery systems.[8] The primary aim of the current study was to synthesize and assess Arabinoxylan (AX)-based nanoparticles loaded with APZ for oral drug delivery.

Materials and Methods

Materials

The maize husk employed in this experimental study was procured from the Chakwal market, Pakistan. A voucher specimen of *Zea mays* (MS-708) has been deposited in the Herbarium (SARGU) of the Department of Botany, University of Sargodha, for future reference and research purposes. The chemicals and reagents used in this study were of analytical grade. Disodium dihydrogen phosphate, potassium dihydrogen phosphate, and dimethyl sulfoxide were obtained from Merck (Germany), while hydrochloric acid (HCl), sodium chloride (NaCl), methanol, ethanol, and acetonitrile were procured from Supelco (USA). Sodium hydroxide (NaOH) was obtained from Sigma-Aldrich (USA) and Merck (Germany). Aripiprazole (APZ) was generously provided by Genome Pharmaceuticals (Rawalpindi).

Method

Alkali Extraction of AX by Autoclave Treatment

Arabinoxylan was extracted from the dried ground maize husk using 1% sodium chloride solution as reported by Valério et al, 2021 with slight modifications as shown in Figure 1.[9] A total of 10 grams of ground maize husk were precisely weighed and transferred to a 500 mL flask, where a 1% alkali solution was added at a solid-to-liquid ratio of 1:10. The bottle was sealed with lids and placed into an autoclave. The sample was autoclaved at 121°C and 15 lbs pressure for 60 min. The slurry was obtained followed by its pH adjustment to 5 using glacial acetic acid. The entire slurry was initially filtered through muslin cloth. The solid residue was discarded, and the filtrate was retained. The retained sample was then mixed with ice-cold rectified alcohol (1:3) resulting in precipitation and put at 4°C overnight. It was subsequently filtered again using filter paper to collect the solid precipitates, which were then washed with a 1:1 mixture of acetone and 95% ethanol. The obtained residue was AX, which was subjected to drying at 60 ± 2°C. After drying, the obtained AX sample was milled using a grinder-mixer and stored at room temperature until further study.[10] Figure 1 illustrates a stepwise process of AX extraction, depicting each stage involved in the extraction procedure.

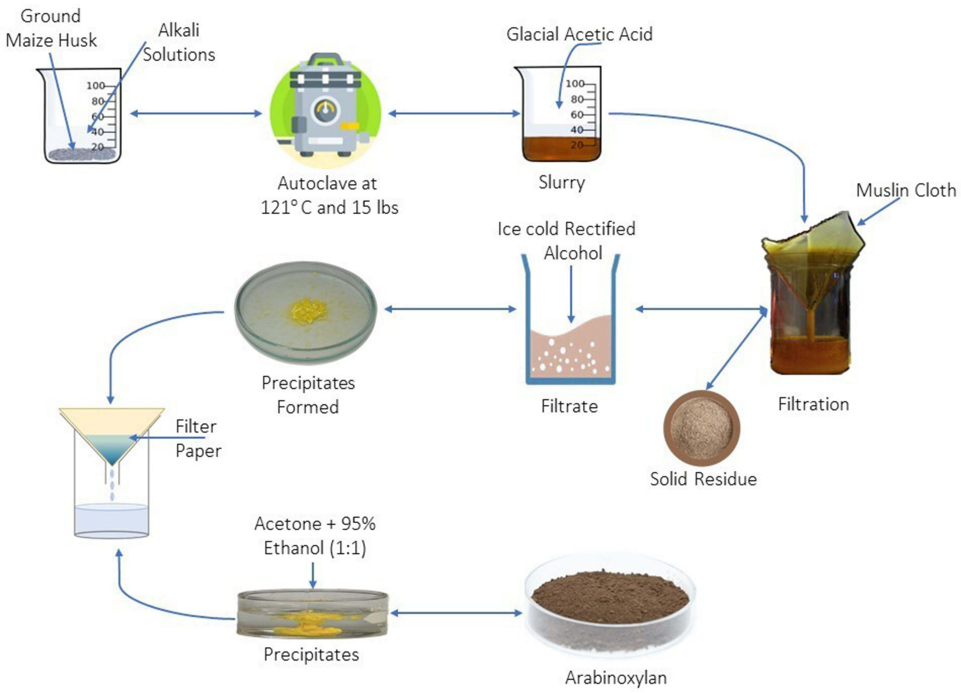

Figure 1 Pictorial representation of stepwise AX extraction.

Characterization of AX

Percentage Yield

The percentage yield of AX obtained can be estimated by Equation 1 given below:[11]

$$\%\text{Yield} = \left(\frac{x}{y}\right) \times 100 \tag{1}$$

Where:
% yield represents the percentage yield of AX
x represents the weight of AX
y represents the weight of corn husk

Micromeritics

Flowability of ground AX was determined by measuring the angle of repose, Hausner ratio and Carr's index. The angle of repose was measured using the fixed funnel method, while the Hausner ratio and Carr's index were calculated from the bulk and tapped densities of the samples.

Angle of Repose

Fifty grams of powder was poured through a funnel onto a sheet of paper to form a conical pile. At the end of the experimental run, the mean diameter (2R) of the powder cone's surface was measured, and the angle of repose was calculated using Equation 2:

$$Tan\ \alpha = H/R \tag{2}$$

where α is the angle of repose. Process was repeated three times, and their average was reported as the angle of repose.[12,13]

https://doi.org/10.2147/NSA.S502002

Bulk Density

Bulk density was measured by modifying the method described in the United States Pharmacopeia (USP). A 100 mL graduated cylinder with 0.5 mL markings was tared on a weighing balance and filled with powdered arabinoxylan without compaction until 100 mL. The volume recorded was considered the apparent volume (V_O). Bulk density (ρ_{bulk}) was measured by dividing the powder weight by the apparent volume for the powder run. Bulk density was measured thrice.[14] Equation 3 for determining bulk density is given by:

$$\rho_{bulk} = m/V_O \tag{3}$$

Tapped Density

A graduated cylinder was tapped 50 times, and the final volume of the powder (V_f) was recorded. Tapped density (ρ_{tapped}) was determined by dividing the powder weight by the final volume. Tapped density measurements were taken three times for each powder run.[15] Equation 4 for tapped density evaluation is as follows:

$$\rho_{tapped} = \mathrm{M}/\mathrm{V_f} \tag{4}$$

Compressibility Index & Hausner Ratio

Compressibility Index & Hausner ratio were determined as per USP guidelines to predict the powder flow properties. Both parameters were recorded using measured values for bulk density and tapped density and were recorded thrice for experimental run. Equation 5 and Equation 6 for calculating the Compressibility Index & Hausner ratio are given as under:

$$Compressibility\ Index = \left[\left(\rho_{tapped} - \rho_{bulk}\right)/\rho_{tapped}\right] \times 100 \tag{5}$$

$$\text{Hausner's ratio} = \frac{\rho_{tapped}}{\rho_{bulk}} \tag{6}$$

Preparation of APZ-Loaded AX Nanoparticles by Ionotropic Gelation Method

AX-based nanoparticles containing APZ were synthesized by ionotropic gelation technique using barium chloride being a cross-linker.[16] The entire composition of AX-based nanoparticles containing APZ is shown in Table 1. Initially, solution A was prepared by dissolving a desired concentration of AX in distilled water, resulting in a 5 mg/mL solution under continuous stirring with gentle heat on a hot plate magnetic stirrer set at 500 rpm.

Table 1 Composition of AX-Based Nanoparticles Containing APZ

Nanoparticles code	Drug (APZ) mg	Polymer (AX) mg	Cross-linker ($BaCl_2$) %
FN1	10	20	5
FN2	10	30	5
FN3	10	40	5
FN4	10	50	5
FN5	10	20	2
FN6	10	20	3
FN7	10	20	4

Then, the known concentration of APZ was dissolved in dimethyl sulfoxide (2% v/v), resulting in a clear solution at the concentration level of 1mg/mL obtaining a solution of concentration 1mg/mL APZ under continuous stirring to obtain a clear solution. This solution was named solution B. Consequently, solution C was prepared by dissolving various concentrations of barium chloride into the distilled water. Both solution A and solution B were mixed with each other and left under continuous stirring to obtain a homogeneous solution. Phosphoric acid was used to adjust the pH of the resultant solution to 4.5. This resulting solution was filled into a 20-gauge syringe needle and was added dropwise under magnetic stirring to the barium chloride solution (solution C) at room temperature for 60 minutes. Opalescent dispersion was obtained and centrifuged (sigma 3K30, Osterode, Germany) at 12,000 rpm/30 min. Nanoparticles formed and were settled down at the bottom. They were further lyophilized at −50°C and were stored at 4°C for further use.[17]

Entrapment Efficiency (EE)

EE of AX-based nanoparticles containing APZ were determined by transferring the final suspension to centrifugation tubes, and centrifugation was done at 15000 rpm for 30 minutes. The supernatant containing unentrapped APZ was collected and measured using a UV spectrophotometer at 259 nm. The amount of entrapped APZ in the nanoparticles was estimated using Equation 7. APZ determinations were performed three times, and the results are presented as averages with standard deviations (SD).[18]

$$EE(\%) = \frac{actural\ drug\ loading}{theoretical\ drug\ loading} \times 100 \tag{7}$$

In-vitro Dissolution and Drug Release Kinetics

An in vitro release study was conducted using the dialysis method.[19] AX-based nanoparticles containing 10 mg of APZ were separately dispersed into 2 mL of dissolution medium (pH 1.2 buffer and pH 6.8 buffer) within a dialysis membrane (D9402-100FT; Sigma-Aldrich, Steinheim, Germany) with a molecular weight cutoff of 12,000 Da. Dialysis bag was sealed and placed into 100-mL of the same release medium under continuous stirring at 75 rpm, maintaining the temperature at 37°C. Drug release study was performed for 24 hours. Samples of 2 mL were taken out at definite time intervals of 1, 2, 3, 4, 5, 6, 8, 12, and 24 h and restored by the same volume of fresh release medium. Sample aliquots containing the amount of APZ released from the nanoparticles were filtered and assessed by UV spectrophotometric analysis at 259 nm. The calibration curves of APZ at both pH 1.2 and pH 6.8 were plotted to determine the drug concentration.[20] AX-based nanoparticles containing APZ were further investigated by applying kinetic models including Zero order, First order, Higuchi, Korsmeyer-Peppas, and Hixson-Crowell models via DD Solver, release profiles were assessed.[21]

Characterization of Optimized Nanoparticles

Particle Size, Polydispersity Index and Zeta-Potential

Using Dynamic Light Scattering (DLS), the average particle size and size distribution were determined (Brookhaven Instruments Corporation, Holtsville, NY, USA). The same device was used to estimate the surface charge of the particles by measuring the zeta potential. Particle size, surface charge, and zeta potential values were measured for each sample at 25°C, yielding an average of three readings.[22]

Fourier-Transform Infrared Spectroscopy (FTIR)

Fourier Transform Infrared (FTIR) analysis was performed to identify the functional groups in the samples and analyse their molecular composition and structure. FTIR analysis of all the samples, including APZ, AX, and nanoparticles, was conducted using the potassium bromide pellet method. This method involved grinding the sample into a fine powder and dispersing it in KBr at a 1:100 ratio by weight. The mixture was then compressed in a mold for 5 minutes before being placed into the spectrophotometer for transmission analysis. The spectra were recorded from 4000 to 400 cm^{-1} wavenumber.[23,24]

Scanning Electron Microscopy (SEM)

The surface morphology of nanoparticle formulation was determined by scanning electron microscopy (JSM-7610 F, JEOL). Dried nanoparticles weighing approximately 1 mg were transferred onto a sample disk using carbon adhesive. The nanoparticle samples were then coated with chromium. After coating, the disk was fixed onto the sample holder and placed inside the sample compartment of the scanning electron microscope (SEM). Micrographs were recorded at a pressure of 10 Pascal in the sample compartment. The SEM features an electron gun operating at a filament current of 60 μA and an accelerating voltage of 25 kV.[18]

Thermal Analysis

Thermal analysis was carried out of pure APZ powder, pure arabinoxylan powder, and nanoparticles by using a Thermogravimetric Analyzer model SDT Q 600 Series Thermal Analysis System (TA instruments, New Castle DE, UK) from room temperature to 600°C. The samples were ground and passed through mesh 40. A dry sample weighing 5–10 mg was placed in an open platinum pan attached to a microbalance. A heating rate of 10°C/min was applied under a nitrogen atmosphere with a flow rate of 20 mL/min. All measurements were performed in triplicate.[25]

Powder X-Ray Diffraction (PXRD)

The XRD data of the samples were collected using an X-ray diffractometer (Philips X-ray Analytical, Amsterdam, The Netherlands) with a Cu-sealed tube. The instrument operated at 40 kV and 20 mA, with a stability of 0.01% over 8 hours. Measurements for each sample were recorded in the scattering 2θ range of 5° to 70°, with a step size of 0.04° and a count rate of 5 seconds per step.[26]

Ex-Vivo Intestinal Permeation Study

Everted intestinal sac method with mild adaptations was carried out on male Wistar rats (weighing 180–210 g) for the permeation study of APZ from nanoparticles. The whole experimental protocol was approved by the Institutional Animal ethical committee (Pharmacy Research Ethics Committee, PREC/05/19) of the Capital University of Science and Technology (CUST) Islamabad, Pakistan. The study was conducted in strict accordance with internationally recognized animal welfare standards, including the National Institutes of Health (NIH) Guide for the Care and Use of Laboratory Animals, which provide comprehensive guidance on the ethical and humane treatment of research animals. The drug permeation study was conducted at pH 1.2 (SGF) as well as at pH 6.8 (SIF) for 24 hours. Abdominal hair of rats was removed using an electric razor and electric clipper one day before the permeation study. Rats were anaesthetized for surgery using chloroform and decapitated. The abdominal skin was cut off immediately.[27] Surgery on the rat was performed by cervical dislocation, followed by a midline abdominal incision to access the abdominal cavity. The intestinal segment (colon) was carefully removed and then cleaned with an isotonic solution. A thin glass rod was inserted into one open end of the colon, and the segment was gently rolled down over the rod.

One end of the colon was knotted and a prepared nanoparticle suspension containing 10 mg of equilibrated APZ was injected into the colon sac using the hypodermic syringe needle, and the other end was fastened in the same way to make a closed sac. The filled colon segment was immersed into different beakers containing 100 mL of SGF and 100 mL of SIF. The conical flasks were placed in thermostatic water baths maintained at 37 ± 0.5°C. At regular intervals, a 1 mL aliquot was withdrawn and replaced with an equal volume of fresh medium. These samples were then analysed using a UV spectrophotometer at 259 nm.[28]

Acute Oral Toxicity Study

Acute oral toxicity study was conducted in male Wistar rats (250–260 g). This study adhered to the Organisation for Economic Co-operation and Development (OECD) Guidelines for the Testing of Chemicals, Section 4: Health Effects, Test No. 423: Acute Oral Toxicity – Acute Toxic Class Method (OECD, 2001), which provides a standardized approach for evaluating acute toxicity after oral exposure in laboratory animals. The rats were administered APZ-loaded AX-based nanoparticles orally at a dose of 5000 mg/kg of body weight.[29] They were observed daily for 14 days for any signs of mortality, illness, reactions to the treatment, and changes in mucous membranes, eyes, skin, fur, behaviour, salivation,

diarrhoea, tremors, sleep, or coma. Rat body weights were recorded on the 1st day (before starting the study), the 3rd day, the 7th day, and the 14th day. Food and water consumption was also evaluated on these days and compared with controls. On the 14th day, at the end of the experimental study, the rats were sacrificed under chloroform anaesthesia, and blood was withdrawn from the posterior vena cava through cardiac puncture.

Blood was transferred to sampling vials for haematological analysis. Blood serum was also subjected for renal and lipid profile.[30] All rats were sacrificed at the end of the experimental study. Organs ie, heart, kidney, Spleen, liver, lung, brain and stomach were immediately isolated. These were examined thoroughly for detecting any abnormality and washed using normal saline. The tissue samples were fixed in 10% (v/v) buffered formalin for 24 hours for histopathological analysis. For morphological examination, photomicrographs were captured 40 × magnification.[31]

Pharmacokinetic Studies in Rabbits

Pharmacokinetic parameters of AX-based nanoparticles loaded with APZ were determined in the plasma of 18 male white rabbits (1.5–2 kg), housed in the animal facility at the Faculty of Pharmacy (FOP), Capital University of Science and Technology (CUST). Food was withheld 12 hours prior to the experimental investigation. The rabbits were randomly divided into two groups, each with nine animals (n = 9). The study design for pharmacokinetic analysis is presented in Table 2. Rabbits in both groups received oral doses via an intragastric tube.[32]

A 2 mL blood sample was collected retro-orbitally at the following time points:

0 (pre-dosing), 1, 2, 3, 4, 6, 10, and 24 h post-treatment. The plasma was separated by centrifugation and frozen at −20°C until further analysis.[33] The analysis was conducted using an Agilent Technologies 1200 Series HPLC system with an Agilent 4.6 × 150 mm, 5 µm column. A mobile phase consisting of a 35:65 (v/v) mixture of acetonitrile and triethanolamine buffer was used. Detection was performed at 254 nm with a UV detector, using a 10 µL injection volume.[34] Pharmacokinetic parameters of APZ, including Lambda-z (h^{-1}), half-life ($t_1/_2$), log-time (h), Clast_obs/Cmax, peak plasma concentration (Cmax), and time to reach peak concentration (Tmax), were analysed from plasma levels in rabbits using non-compartmental pharmacokinetic analysis with Kinetica software version 4.4. The area under the plasma concentration–time curve (AUC_{0-t}) was computed using the trapezoidal rule.[35]

Statistical Analysis

All experiments were conducted in triplicate, and the results are presented as the mean ± standard deviation (SD). Statistical analyses were performed using OriginPro 2023. A one-way analysis of variance (ANOVA) was used to analyse data from entrapment efficiency (EE), in-vitro dissolution, and ex-vivo intestinal permeation studies, with a significance threshold set at $p < 0.05$. For two-group comparisons, such as those in acute toxicity and pharmacokinetic studies, statistical significance was evaluated using an independent *t*-test.

Results and Discussion

Percentage Yield

The proportion of the husk's total mass was calculated as AX. Yield of AX extracted through first method (Alkaline Extraction of AX by autoclave) was greater ie, 42% as compared to second method (Extraction of AX using centrifugation) ie, 19%. The existence of lignin residuals, which may retain some hemicelluloses and prevent their extraction, may cause comparatively low percentage yields. Hemicelluloses are often ester linked to lignin via acetyl

Table 2 Experimental Design for Pharmacokinetic Analysis in Rabbits

Groups	Dose Administration to rabbits
Group I	2 mL of normal saline was given orally to the rabbits containing APZ 10 mg/kg body weight.
Group II	The rabbits were given an oral dose of 2 mL of normal saline containing AX based nanoparticles loaded with APZ, at a dose of 10 mg/kg body weight.

https://doi.org/10.2147/NSA.S502002

groups and p-hydroxycinnamic acid, which prevents the hemicelluloses from being released from the matrix to be removed. No technique has yet been established to extract all hemicelluloses from lignocellulosic materials selectively, with high yield and purity levels, and without significant degradation.[36]

Micromeritics

The micromeritics parameters of AX demonstrated that AX exhibited good flowability. The angle of repose of powdered AX was found to be 32.42 ± 0.03 exhibiting good flow. The results of bulk density and tapped density were recorded to be 0.814 ± 0.006 cm^3 /mL and 0.972 ± 0.003 cm^3 /mL respectively. The values of Hausner´s ratio 1.19 ± 0.023 and Carr´s index was calculated to be 16.25 ± 0.700 illustrating the fair flow. A material's capacity to flow and reorganise under compression increases with its higher bulk and tapped densities. The findings displayed here indicated that the angle of repose, Carr's index, and Hausner's ratio were all within acceptable ranges. When powdered material encounters the carrier, its free-flowing characteristics ensure a large surface area and prevent particle agglomeration, enabling the particles to diffuse quickly and disperse readily. These outcomes would speak to the dried powder's ability to entrap the drug.[37]

Entrapment Efficiency (EE)

The molecular weight of arabinoxylan (AX) is an essential factor influencing the polymer's ability to encapsulate drugs. Higher molecular weight polymers possess longer chain lengths, which promote greater intermolecular interactions and a more robust polymer network. This leads to the creation of a more compact matrix, which can trap and retain the drug more effectively, thereby increasing the entrapment efficiency. Conversely, polymers with lower molecular weights may form less dense matrices, reducing the entrapment capacity and stability of the nanoparticles. The results presented in Table 3 show that the encapsulation efficiency (EE) of nanoparticle formulations FN1, FN2, FN3, and FN4 increased from 58.3% ± 0.90 to 88.9% ± 1.77. This improvement can be attributed to the higher polymer concentration, which, in turn, influences the molecular weight of the polymer network. A higher polymer concentration generally results in an increase in the molecular weight of the polymer chains, leading to longer and more entangled chains. These longer chains create a denser and more cohesive polymer matrix, which restricts the diffusion of the drug into the surrounding medium. This reduced drug diffusion enhances the encapsulation efficiency (EE) by preventing the drug from leaching out during nanoparticle formation. Consequently, the higher molecular weight of the polymer in thicker formulations effectively limits drug penetration and increases the overall EE. Conversely, the entrapment efficiency (EE) of nanoparticle formulations FN5, FN6, and FN7 increased from 43.4% ± 0.52 to 53.13% ± 0.84 with a rise in cross-linker concentration, as shown in Table 3. This increase may be attributed to the fact that a low concentration of cross-linker produces a loose polymer matrix with large pores due to insufficient cross-linking. Consequently, the drug leaches into the cross-linker solution, resulting in lower entrapment efficiency. This discussion underscores a direct relationship between entrapment efficiency (EE) and cross-linker concentration. Among all nanoparticle formulations, FN4 stands out as the optimal formulation due to its highest EE compared to the others. This formulation achieves its optimal EE through the precise concentrations of AX and

Table 3 Entrapment Efficiencies of Formulations (Mean ± SD, n = 3)

Formulations code	Drug (APZ) mg	Polymer (AX) mg	Cross-linker ($BaCl_2$) %	Entrapment efficiency %
FN1	10	10	5	58.3 ± 0.90
FN2	10	20	5	65.1 ± 1.47
FN3	10	30	5	72.3 ± 1.69
FN4	10	40	5	88.9 ± 1.77
FN5	10	20	2	43.4 ± 0.52
FN6	10	20	3	48.43 ± 1.03
FN7	10	20	4	53.13 ± 0.84

the cross-linker, leading to a dense polymer matrix and a thick solution. These factors collectively reduce drug diffusion into the barium chloride solution, thereby enhancing EE.[38] Significant differences were observed between formulations FN1, FN2, FN3, and FN4, with FN4 showing the highest EE (88.9% ± 1.77), indicating that increasing the polymer concentration led to a significant enhancement in EE ($p < 0.05$). Additionally, formulations FN5, FN6, and FN7, which varied by cross-linker concentration, showed a moderate increase in EE, with FN7 achieving the highest EE in this group (53.13% ± 0.84), reflecting a significant impact of cross-linker concentration on EE ($p < 0.05$).

In-vitro Dissolution Test

The dissolution profiles of all seven nanoparticle formulations, obtained using the USP dissolution apparatus type II (Pharma Test, Hainburg, Germany), are presented in Figures 2A and B. Simulated gastric fluid (SGF) and simulated intestinal fluid (SIF) were the two media utilized for the dissolution studies. The results indicated that the release of each formulation was pH-dependent, with higher dissolution rates observed in SIF. This enhancement may be attributed to the greater solubility of APZ at basic pH compared to acidic pH. In acidic conditions, nanoparticle formulations FN1-FN7 exhibited dissolution percentages of 44.28%, 36.74%, 30.27%, 25.85%, 23.65%, 18.33%, and 14.75%, respectively, over a 24-hour period. Drug release was significantly influenced by both polymer and cross-linker concentrations. Specifically,

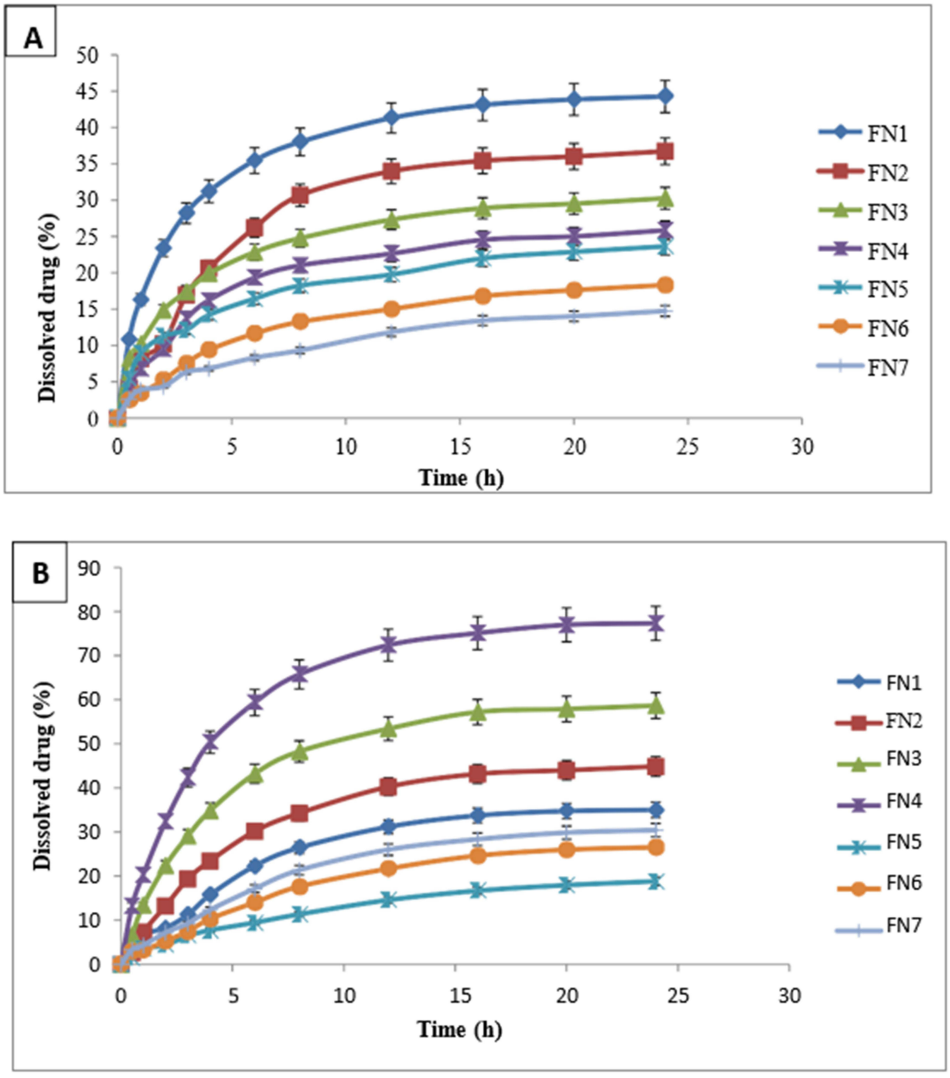

Figure 2 In vitro release profile of APZ-loaded AX Nanoparticles **(A)** SGF **(B)** SIF.

https://doi.org/10.2147/NSA.S502002

as the polymer concentration increased, drug release decreased; a similar trend was observed with cross-linker concentration. The slower dissolution in acidic medium could be due to factors such as polymer swelling, slow polymer degradation, or the low solubility of APZ at acidic pH. Conversely, in SIF, nanoparticle formulations FN1-FN7 demonstrated dissolution percentages of 35.01%, 44.87%, 58.67%, 77.33%, 18.83%, 26.55%, and 30.44% over the same 24-hour period. Notably, the study revealed that in SIF, there was an exponential release during the initial hours, followed by a constant release rate thereafter. For instance, the FN4 formulation exhibited an exponential release of 65.747% in the first 8 hours, after which the release rate stabilized.[39] Statistical analysis of the dissolution profiles was performed using one-way analysis of variance (ANOVA) to compare the dissolution rates between the formulations in both SGF and SIF. The results revealed statistically significant differences in the dissolution rates between formulations ($p < 0.05$), with FN4 and FN3 showing notably higher release percentages compared to FN1 and FN2 in SIF. Post-hoc Tukey's test confirmed that these differences were highly significant, particularly in the SIF medium, where formulations with higher polymer concentrations and cross-linker ratios (FN4) exhibited the most favourable dissolution profiles. These findings underscore the critical role of formulation components in controlling drug release, with FN4 demonstrating the most robust release characteristics and positioning it as the optimal formulation for enhancing the solubility and bioavailability of APZ under physiological conditions.

To analyze the release kinetics, the drug release curves were fitted to five distinct mathematical models, and the correlation of each model with the experimental data is detailed in Table 4. Kinetic analysis using SGF as the dissolution medium revealed that all formulations (FN1-FN7) conformed to the Korsmeyer-Peppas model. Specifically, formulations FN1-FN6 had a diffusion exponent (n) of less than 0.45, indicative of Fickian diffusion, while FN7 exhibited an n value of 0.45, suggesting a transition to anomalous diffusion. In SIF, the release profiles similarly followed the Korsmeyer-Peppas model. All formulations displayed Fickian diffusion with diffusion exponents (n) less than 0.45, except for FN7,

Table 4 Correlation Coefficients (R^2) and Release Rate Constants of APZ-Loaded APZ-Based Nanoparticles (A) SGF and (B) SIF

(A) Summarized Data in SGF											
	Zero order		**First order**		**Higuchi**		**Korsmeyer Peppas**			**Hixson-Crowell**	
	R^2	**K_0**	**R^2**	**K_1**	**R^2**	**kH**	**R^2**	**kKP**	**N**	**R^2**	**kHC**
FN1	0.0228	1.738	0.1840	0.022	0.8324	7.498	0.9799	12.302	0.303	0.7548	0.008
FN2	0.2994	1.462	0.4322	0.018	0.9044	6.228	0.9580	8.748	0.366	0.7198	0.011
FN3	0.4845	2.087	0.6519	0.028	0.9292	8.784	0.9447	10.756	0.421	0.6386	0.017
FN4	0.1573	2.603	0.2121	0.040	0.7768	11.311	0.9931	3.374	0.445	0.7454	0.037
FN5	0.6072	0.781	0.6548	0.009	0.9862	3.243	0.9637	19.384	0.286	0.8166	0.003
FN6	0.1180	1.319	0.2530	0.016	0.8779	5.643	0.9901	8.821	0.323	0.8481	0.005
FN7	0.5992	0.991	0.6618	0.011	0.9723	4.126	0.9778	4.683	0.450	0.8113	0.006
(B) Summarized Data in SIF											
	Zero order		**First order**		**Higuchi**		**Korsmeyer Peppas**			**Hixson-Crowell**	
	R^2	**K_0**	**R^2**	**K_1**	**R^2**	**kH**	**R^2**	**kKP**	**N**	**R^2**	**kHC**
FN1	0.6738	1.937	0.1840	0.022	0.8324	7.498	0.9799	12.302	0.303	0.7548	0.008
FN2	0.5946	2.505	0.4322	0.018	0.9044	6.228	0.9580	8.748	0.366	0.7198	0.011
FN3	0.3935	3.357	0.6519	0.028	0.9292	8.784	0.9447	10.756	0.421	0.6386	0.017
FN4	0.2277	4.493	0.2121	0.040	0.7768	11.311	0.9931	3.734	0.445	0.7454	0.037
FN5	0.7877	0.972	0.6548	0.009	0.9862	3.243	0.9637	19.384	0.286	0.8166	0.003
FN6	0.8068	1.404	0.2530	0.016	0.8779	5.643	0.9901	8.821	0.323	0.8481	0.005
FN7	0.7549	1.637	0.6618	0.011	0.9723	4.126	0.9778	4.683	0.450	0.8113	0.006

which had an n value of 0.45. This consistency in the release mechanism across different pH conditions underscores the robustness of the Korsmeyer-Peppas model in describing the drug release kinetics.[40]

Statistical analysis was performed to ensure the robustness of the data. Among the seven formulations, FN4 was identified as the optimized formulation based on its superior entrapment efficiency and dissolution profile. This formulation demonstrated the most favorable characteristics and was selected for further investigation.

Table 4 presents the Correlation Coefficients (R^2) and Release Rate Constants (k) for APZ-loaded AX-based nanoparticles in both (A) SGF and (B) SIF. The table illustrates the outcomes of applying different kinetic models, with the k values representing the release rate constants. The results indicate that the release of APZ from AX-based nanoparticles is governed by diffusion, suggesting that these nanoparticles could serve as an effective system for providing prolonged drug release.[41]

Characterization of Optimized Nanoparticle Formulation

Mean Particle Size, Zeta Potential, and Polydispersity Index (PDI)

The size distribution of the FN4 formulation is presented in 3(A), which demonstrates the range of the particle sizes. The zeta potential of the FN4 formulation is provided, 3(B), indicating the surface charge and stability of the nanoparticles. Particle size reduction is one of the most commonly used approaches to increase surface area to enhance the dissolution rate.[42] The particle size and mean polydispersity index of the optimized FN4 formulation were measured immediately after precipitation using dynamic light scattering (Zetasizer). Figure 3A shows that the mean particle size of formulation FN4 was recorded at 284.4 nm. The formulation exhibited a narrow distribution, evidenced by a polydispersity index of 0.346. This narrow distribution is advantageous as it helps mitigate issues associated with the variable solubility of drug

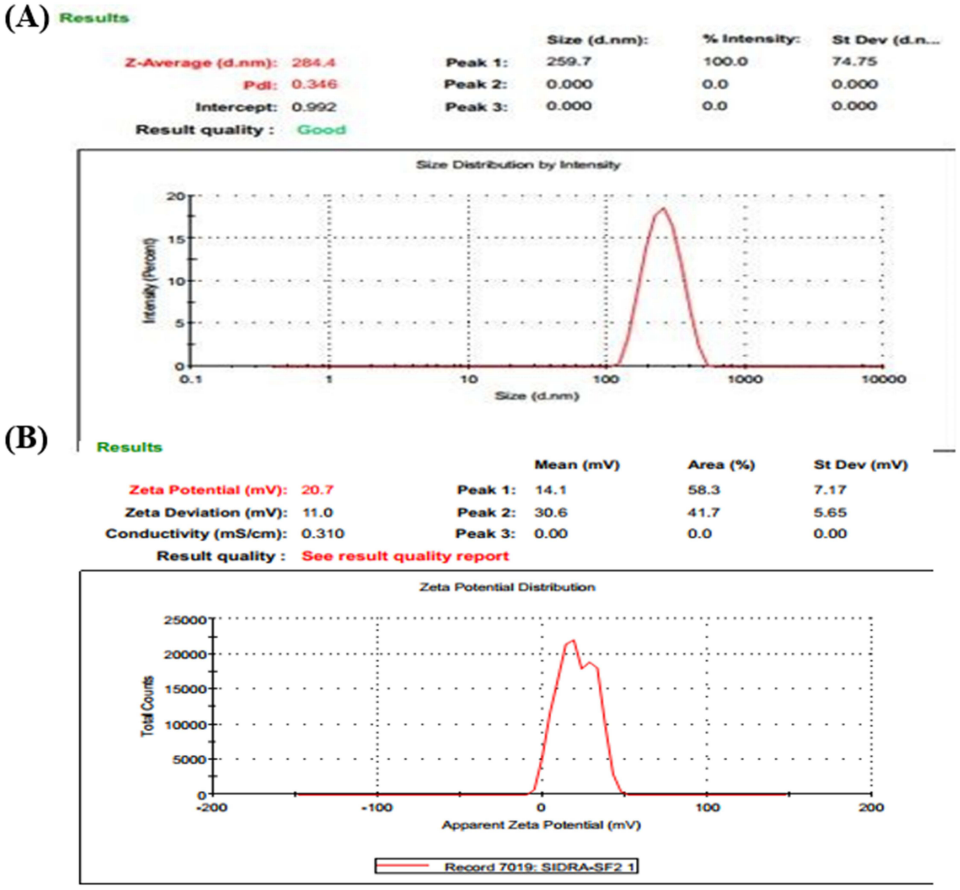

Figure 3 (A) Size distribution of FN4 formulation **(B)** Zeta potential of FN4 formulation.

https://doi.org/10.2147/NSA.S502002

particles of different sizes, thereby contributing to long-term stability.[43] The significant reduction in particle size enhances the dissolution rate and oral bioavailability. Figure 3B shows that the zeta potential of APZ nanoparticles was 20.7 mV, indicating the stability of the nanoparticle formulation. Generally, a zeta potential of approximately ±30 mV is considered the minimum requirement for the stability of nanoparticle dispersions.[44] The lower value of zeta potential might provide electrostatic repulsion preventing the formulation from agglomeration and aggregation of drug nanoparticles. Strong electrostatic interlinkage between AX and the mucus membrane means that mucoadhesion is substantially more prominent in nanoparticles with a positive zeta potential. On mucus membranes, this kind of interaction is beneficial for robust adhesion.[45]

FTIR

Figure 4 shows the FTIR scans of AX, APZ and optimized FN4 formulation. Figure 4A–4C shows the FT-IR spectrum of AX interpreting it's the principal functional groups causing the qualitative chemical description of the polymer. Absorption band at 1041.56 cm^{-1} falls into the polysaccharide region and indicates C-OH linkage. Stretch at 1537.27 and 1674.21 cm^{-1} indicate amide II and amide I linkages, respectively, representing the protein group. Absorption band at 2247.07 cm^{-1} shows the C≡N linkage indicating the nitrile group. Absorption bands at 2983.88 cm^{-1}, 3039.81, and 3118.90 cm^{-1} belong to O-H bond indicating the carboxylic acid. Signals at 3531.66 cm^{-1} indicate the O-H stretching of

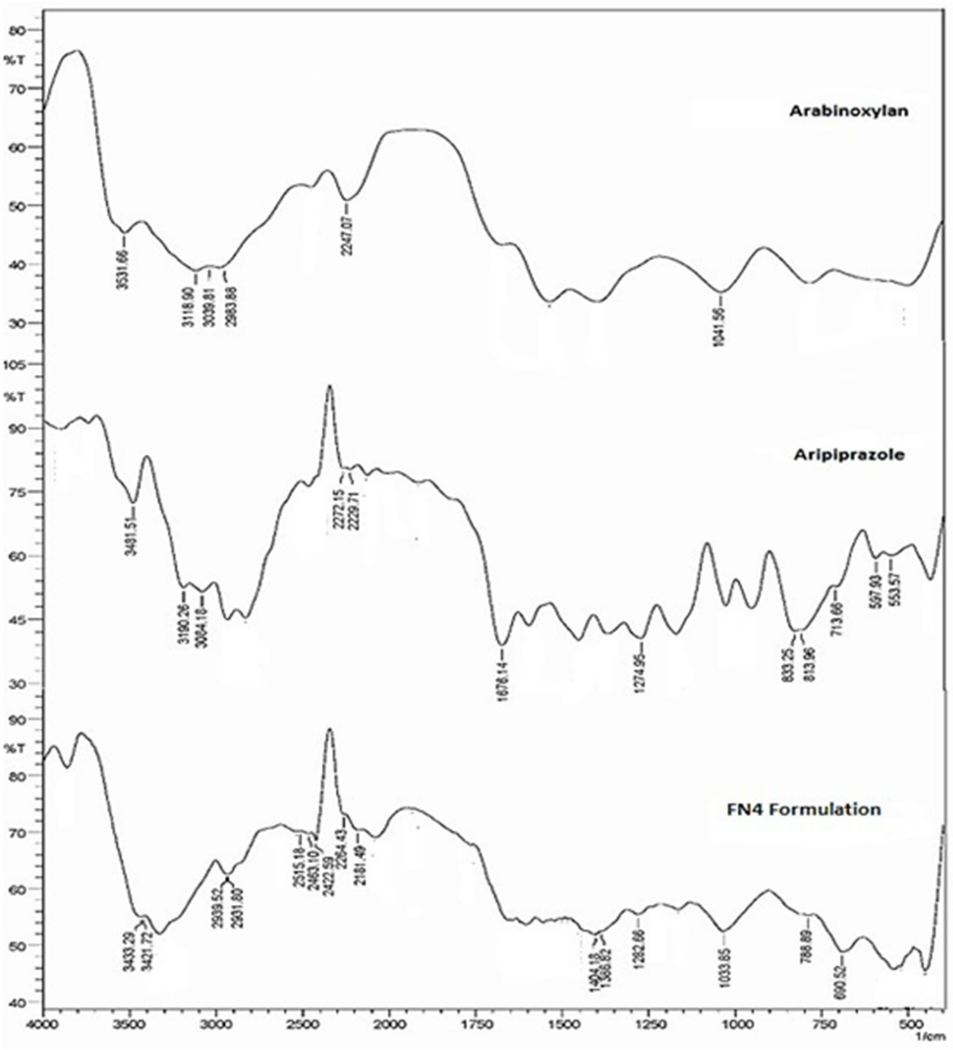

Figure 4 FTIR of Arabinoxylan, Aripiprazole and FN4 formulation.

the alcohol group.[46] The FTIR Spectra of pure APZ shown in Figure 4 indicated sharp peaks representing distinct functional groups in APZ. Absorption bands of APZ at 3190.26 cm^{-1}, 3481.51 cm^{-1} show N-H Stretching. APZ showed C-H aromatic region at 3084.18. Vibration band at 2937.59 cm^{-1} is due to C-H aliphatic stretching and vibration bands.at 2229.71 and 2272.15 cm^{-1} indicate C=N (nitrile group). Intense peak at 1676.14 cm^{-1} showed amide group (N–C=O). Peak at 1274.95 cm^{-1} attributed to aromatic C-O vibration. Absorption bands at 553.57 cm^{-1}, 597.93 cm^{-1}, 713.66 cm^{-1}, 813.96 cm^{-1}, 833.25 cm^{-1} showed the C-Cl stretch region.[47] While interpreting the FTIR spectra of formulation (FN4) as shown in Figure 4, it was noticed that some peaks of AX disappeared showing the entrapment of drug into the AX matrix. Several peaks were shifted towards higher or lower frequencies, and some new peaks appeared in the formulation that were entirely different from those of the parent components. Sharp peak of the polysaccharide region at 1041.56 cm^{-1} was shifted to 1033.85 cm^{-1}. Peak of amide I at 1674.21 cm^{-1} was shifted to 1645.28 cm^{-1} and Peak of amide II at 1537.27 cm^{-1} was shifted to 1554.63 cm^{-1}. Peaks of nitrile group had disappeared in the APZ nanoparticle formulation. Peak at 2983.88 cm^{-1} was shifted to 2931.80 cm^{-1} and peak at 3531.66 cm^{-1} was shifted to 3433.29, respectively. The FTIR analysis of FN4 formulation demonstrated that some bands of APZ disappeared indicating the entrapment of the drug within the matrix. Notably, the bands corresponding to the nitrile groups were absent in the nanoparticle formulation. Amide group, which was located at 1676.1 cm^{-1} was shifted to 1645.28 cm^{-1} representing the hydrogen bond formation between APZ and AX. Band at 3481.51 cm^{-1} showing the N-H stretch was shifted to 3433.29 cm^{-1}. Band at 1274.96 cm^{-1} was shifted to 1282.66 cm^{-1} and bands of C-Cl region ie, 713.66 and 813.96 cm^{-1} were shifted towards lower frequencies ie, 690.52 and 788.89 cm^{-1}, respectively.[47]

Scanning Electron Microscopy (SEM)

Figure 5 shows the SEM images of the FN4 formulation at different magnifications providing detailed visual representations of the nanoparticle surface. SEM images revealed that the prepared nanoparticles were discrete and slightly

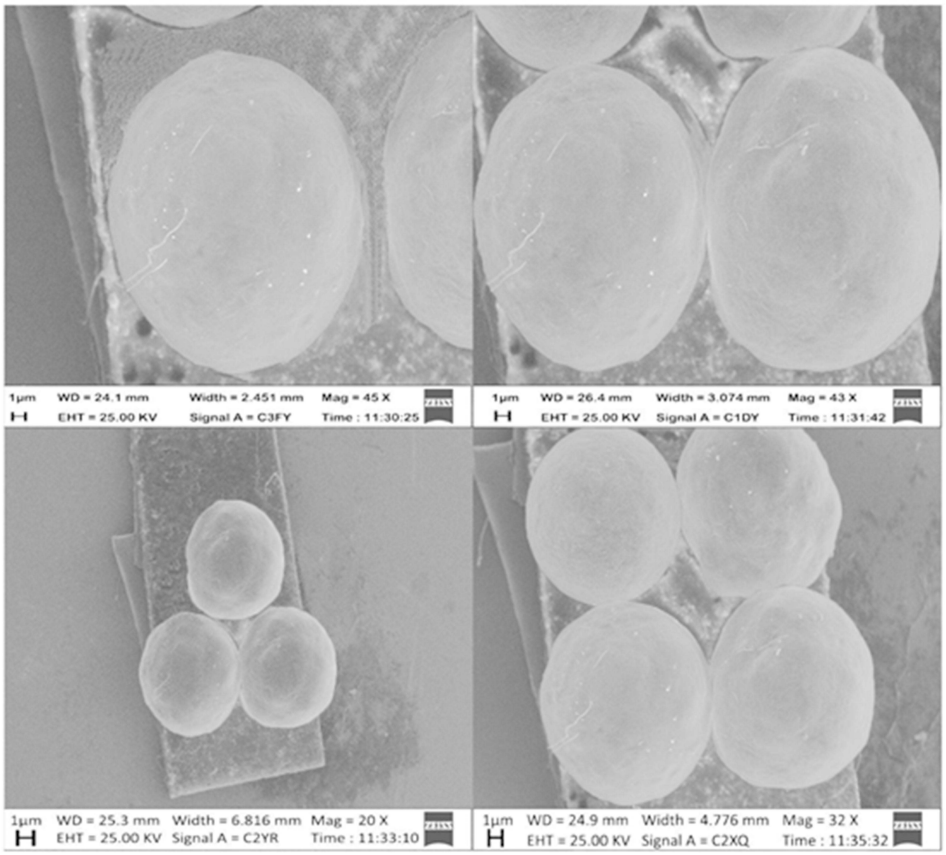

Figure 5 SEM images of FN4 formulation at different magnifications.

https://doi.org/10.2147/NSA.S502002

spherical, exhibiting uniform morphology. Additionally, the SEM analysis indicated a uniform surface with a small number of bright spots. These bright spots on a grey background correspond to pores on the surfaces of the nanoparticles. The porous structure of these nanoparticles is characteristic of polymeric particles formed during the drying of droplets. This phenomenon may be attributed to solvent evaporation, leading to the shrinkage of the polymeric layer on the droplet surface. These pores serve as solvent entry channels, facilitating drug release from the nanoparticles upon contact with an aqueous medium.[48]

Differential Scanning Calorimetry (DSC)

The DSC technique was applied to assess thermal stability AX, APZ, and formulation FN4, as shown in Figure 6A. The DSC thermogram of APZ exhibited an endothermic melting point around 140°C, while AX displayed an endothermic peak at 73.98°C. Notably, the formulation FN4, created by mixing APZ with AX, showed the disappearance of APZ's melting endothermic peak. Additionally, the characteristic peak of AX was also absent, indicating that APZ was efficiently entrapped in the nanoparticles in an amorphous form. Previous literature reports that hydrophobic drugs demonstrate enhanced solubility and bioavailability when in the amorphous state.[49]

Thermogravimetric Analysis (TGA)

Figure 6B illustrates the TGA thermograms of AX, APZ, and formulation FN4, clearly indicating their weight loss due to water loss at various temperatures. APZ decomposes in three stages: a weight loss of 3.46% between 45.41°C and 259.29°C, followed by a significant 66.81% weight loss from 259.29°C to 350.72°C, and finally a 12.75% weight loss from 350.72°C to 383.48°C. In contrast, AX exhibits weight loss across two thermal events: 11.09% from 15°C to 143.54°C, and 56.27% from 143.54°C to 270.4°C. The FN4 formulation, containing APZ-loaded AX nanoparticles,

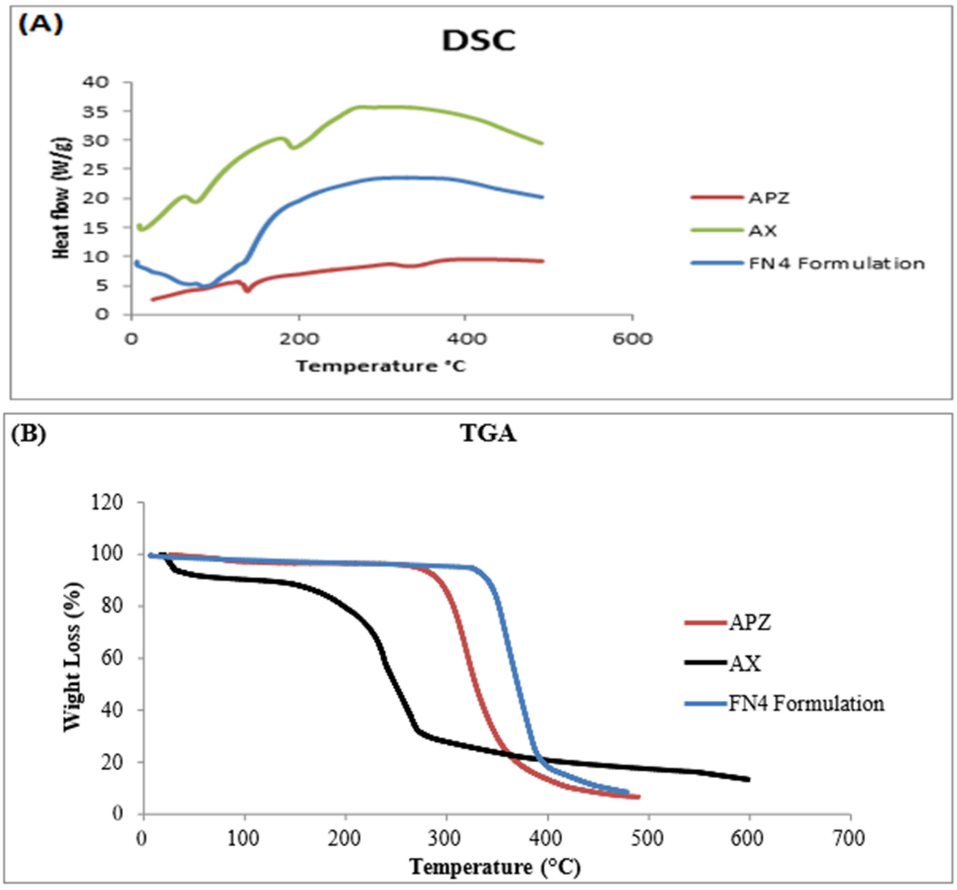

Figure 6 (**A**) DSC thermogram of AX, APZ and FN4 formulation (**B**) TGA pattern of AX, APZ and FN4 formulation.

shows degradation in three stages: 4.05% weight loss from 5.6°C to 90.43°C, 59.85% from 96.43°C to 208.74°C, and 18.49% from 208.74°C to 252.59°C. These results indicate that APZ is effectively encapsulated, contributing to the enhancement of drug stability.[50]

PXRD

Figure 7 presents the PXRD patterns of APZ, AX, and the FN4 formulation. The PXRD pattern of APZ displays sharp peaks at various 2θ degrees, specifically at 19.96°, 23.2°, and 24.68°, along with several secondary peaks, confirming its crystalline state. In contrast, the absence of these sharp peaks in the APZ-loaded AX nanoparticle formulation FN4 indicates successful electrostatic interactions between APZ and AX, resulting in the conversion of APZ from a crystalline to an amorphous state. This transformation is expected to enhance the solubility and stability of APZ, positively influencing both its incorporation and release rate. Furthermore, the purity of the formulations is supported by the lack of additional diffraction peaks that would suggest contamination.[51]

Ex-Vivo Intestinal Permeation Study

The ex vivo intestinal permeation of APZ from APZ-loaded nanoparticle formulations (FN1 through FN7) was investigated using the everted sac method in simulated gastric fluid (SGF) and simulated intestinal fluid (SIF), as illustrated in Figures 8A and B. In SGF, formulation FN4 exhibited the highest cumulative drug permeation at 65.10%, significantly outperforming the other formulations. The permeation rates for the remaining formulations were as follows: FN1 (51.29%), FN2 (46.35%), FN3 (56.28%), FN6 (36.28%), and FN7 (31.75%), with FN5 showing the lowest at 25.64%. One-way analysis of variance (ANOVA) was performed to assess the statistical significance of these differences. The ANOVA results indicated significant differences among the formulations ($p < 0.05$), particularly highlighting that FN4 had a statistically significantly higher permeation compared to FN5 and other formulations.

In SIF, formulation FN4 again demonstrated the highest cumulative drug permeation at 71.99%, which was significantly higher than that of the other formulations. The permeation for the other formulations ranged as follows: FN1 (53.73%), FN2 (59.44%), FN3 (62.32%), FN5 (29.45%), FN6 (40.17%), and FN7 (35.11%).[52] The statistical analysis using ANOVA confirmed significant differences in drug permeation across the formulations ($p < 0.05$), with FN4 showing a statistically significant higher permeation compared other formulations.

The significant differences in drug permeation rates among the formulations underscore the effectiveness of coating APZ nanoparticles with AX, a hydrophilic polymer that enhances drug solubility and increases surface area contact with the mucosal membrane. The nano-size of the particles also contributes to increased permeability through the intestinal tissue, as evidenced by the substantial variations in drug permeation rates among the tested formulations.[53]

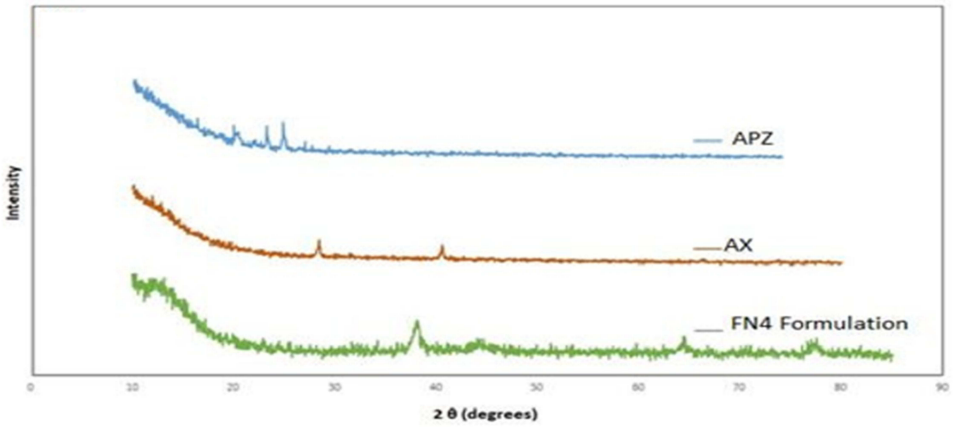

Figure 7 PXRD of APZ, AX and FN4 formulation.

https://doi.org/10.2147/NSA.S502002

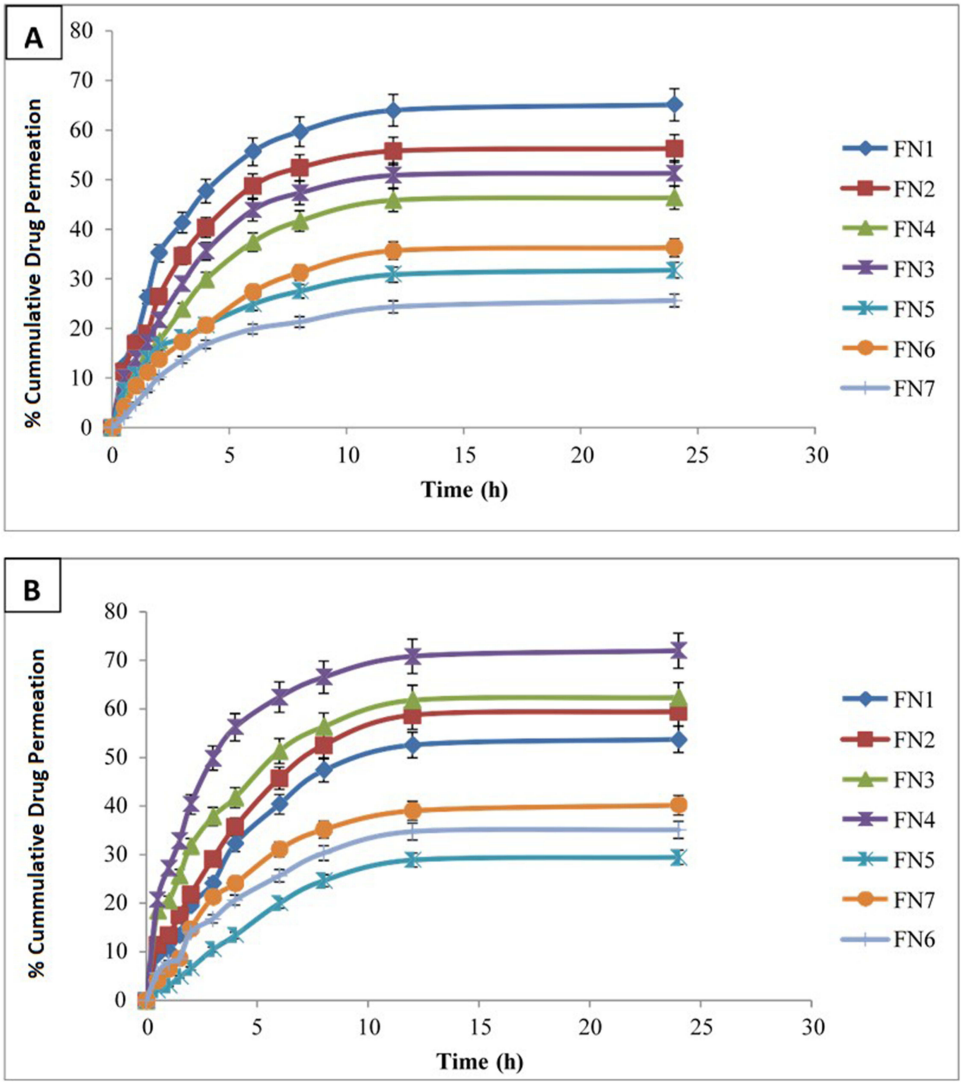

Figure 8 Cumulative Drug Permeation (**A**) SGF (**B**) SIF.

Acute Oral Toxicity Study

The acute oral toxicity levels of male rats treated with the APZ-loaded AX-based nanoparticle formulation FN4 (5000 mg/kg) were evaluated according to OECD guideline 423 over a period of 14 days, with daily observations. Throughout the study, body weights, as well as food and water intake, were recorded, as detailed in Table 5. There was no significant difference in the body weights between the two groups, although Group B exhibited an increase in body weight compared to Group A. Importantly, no treatment-related toxicity or mortality was observed during the evaluation period. Additionally, no adverse conditions such as vomiting, nasal discharge, or eye irritation were reported in any of the rats. Examination of the isolated organs revealed no lesions or abnormalities. Overall, sedation, lethargy, urine color, fur condition, skin appearance, and eye health were all normal.[54] These findings confirm the safety of the FN4 formulation at the tested dose, indicating a lack of acute toxicity and adverse effects. The increase in body weight in Group B, though not statistically significant, suggests normal growth and metabolic health, further corroborated by consistent food and water intake patterns.

Biochemical Blood Investigation of Group A and Group B

The hematological and biochemical parameters of rats from the control (Group A) and treated (Group B) groups were evaluated to assess the pharmacological and safety profile of the nanoparticle formulation FN4. The results are presented in Table 6.

Table 5 Effects on Body Weight, Food Consumption and Water Intake of Rats from Group A and Group B

Observations	Group A	Group B
Signs of illness	No	No
Body Weight (g)		
Day-1	186.0±1.87	199.3±4.01
Day-3	188.0±1.87	200.3±3.64
Day-7	191.5±1.94	203.0±3.83
Day-14	197.0±2.38	209.3±3.45
Food consumption (g)		
Day-1	84.45±1.15	89.85±2.02
Day-3	86.10±1.21	91.10±2.02
Day-7	82.33±1.19	87.50±1.83
Day-14	86.48±0.91	91.18±2.14
Water intake (mL)		
Day-1	209.0±0.88	210.7±1.59
Day-3	212.5±1.19	205.0±1.67
Day-7	206.9±0.73	199.6±1.88
Day-14	214.8±1.01	204.9±1.83

Statistical analysis revealed no significant differences ($p > 0.05$) between the groups for hemoglobin, WBCs, RBCs, platelets, hematocrit, MCV, MCH, MCHC, ALT, AST, total bilirubin, creatinine, urea, uric acid, cholesterol, triglycerides, HDL, and LDL levels. This indicates that the administration of FN4 did not cause substantial alterations in these parameters. These findings suggest that the FN4 formulation is well tolerated and does not induce adverse effects on the hematological or biochemical profiles in experimental animals, supporting its potential for further pharmacological applications.[56]

Table 6 Biochemical Blood Investigation of Group A and Group B

Parameters	Group A	Group B
Hemoglobin (g/dL)	12.65±0.06	12.95±0.12
WBCs (10^3/mm^3)	7.18±0.15	6.40±0.15
RBCs (mL/mm^3)	4.65± 0.06	5.15± 0.13
Platelets (10^3/mm^3)	396.3±1.93	394.0±1.73
Hematocrit (%)	49.75±1.11	48.50±0.65
MCV (Fl)	83.0±2.12	76.50±1.19

(*Continued*)

https://doi.org/10.2147/NSA.S502002

Table 6 (Continued).

Parameters	Group A	Group B
MCH (Pg)	27.25±1.11	26.0±1.23
MCHC (g/dl)	32.5±1.71	33.50±0.65
ALT (U/L)	53.25±0.85	55.50±1.71
AST (U/L)	40.25±1.11	37.0±1.08
Total Bilirubin (mg/dl)	0.65±0.06	0.45±0.03
Creatinine (mg/dl)	0.35±0.06	0.53±0.05
Urea (mg/dl)	34.25±1.11	37.0±1.08
Uric acid (mg/dl)	4.73±0.09	4.68±0.14
Cholesterol (mg/dl)	106.8±0.48	105.0±0.41
Triglyceride (mg/dl)	105.5±0.87	104.3±0.63
HDL (mg/dl)	45.0±1.08	45.50±0.87
LDL (mg/dl)	139.0±0.41	135.8±0.11

Histopathological Examination

Histopathological analysis of the brain, heart, liver, kidney, spleen, lung, and stomach in the FN4-treated groups revealed no abnormalities compared to the vehicle control group, as illustrated in Figure 9. The photomicrographs of the heart showed no lesions in the myocardial fibers for both the control and treated groups. Lung histology exhibited clear alveolar sacs with no evidence of hemorrhage in either group. Liver histology remained intact, demonstrating no significant differences between the groups. However, stomach histology exhibited mild signs of inflammation. Histological assessments of the kidneys and spleen also showed no abnormalities. Additionally, the brains of rats from both the control and treated groups displayed a well-preserved hippocampus, characterized by granular and molecular cell layers.[55] Overall, the histological examination of both the control and treated groups indicated no abnormalities, demonstrating the safety of the AX-loaded APZ nanoparticle formulation FN4.

Pharmacokinetic Parameters

Pharmacokinetic parameters were assessed in healthy rabbits across two groups to compare the performance of an oral APZ suspension and the optimized FN4 nanoparticle formulation. The parameters measured included the elimination rate constant (Lambda-z), half-life ($t_1/_2$), peak plasma drug concentration (Cmax), time to reach peak plasma concentration (Tmax), lag time (Tlag), Clast_obs/Cmax ratio, and the area under the concentration–time curve (AUC_{0-t}).

Plasma concentration data were analyzed using a non-compartmental pharmacokinetic approach with the Kinetica 4.4 software package. The results, summarized in Table 7, revealed significant differences between the two formulations, highlighting the pharmacokinetic advantages of the FN4 formulation.

The FN4 formulation demonstrated a higher Lambda-z (0.053 h^{-1}) compared to the APZ suspension (0.026 h^{-1}), reflecting a faster elimination rate. This was accompanied by an extended half-life ($t_1/_2$) of 13.1924 h for FN4, compared to 8.772 h for the suspension, suggesting prolonged systemic retention. The Tmax for the FN4 formulation was delayed (12 h vs 6 h), indicative of a controlled and sustained drug release mechanism. Moreover, the FN4 formulation exhibited a significantly increased Cmax (742.333 ng/mL vs 235 ng/mL), reflecting improved solubility and absorption, which can be attributed to the enhanced surface area and higher dissolution rate of the nanoparticle formulation.

The AUC_{0-t} for FN4 was nearly double that of the APZ suspension (10,362.749 ng·h/mL vs 5789 ng·h/mL), demonstrating superior bioavailability and a more effective systemic drug delivery profile. The unchanged lag time (Tlag = 0 for both formulations) indicates that the drug's absorption phase was not delayed. The lower Clast_obs/Cmax

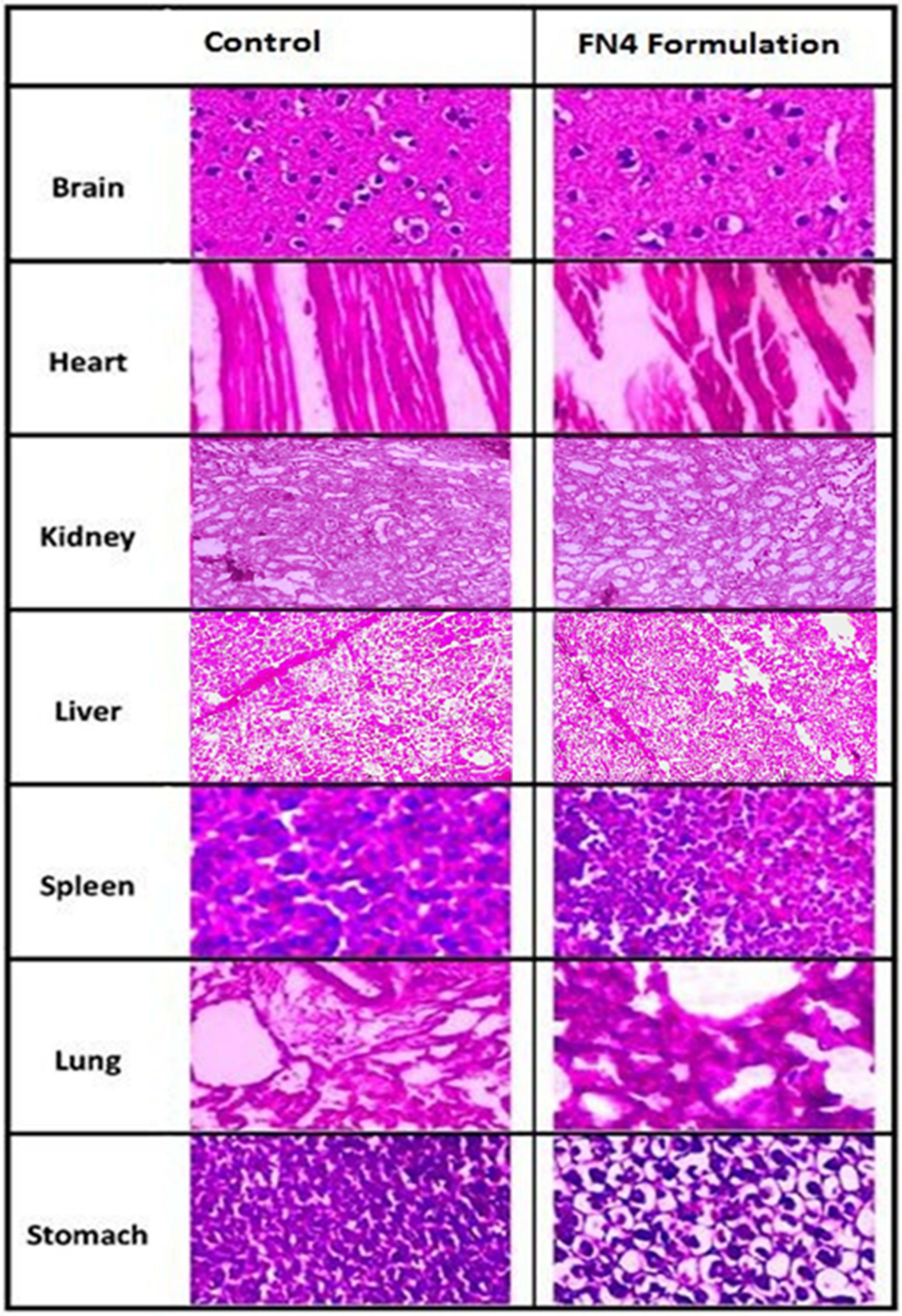

Figure 9 Histopathological Analysis of FN4-Treated Group and Control Group.

ratio for FN4 (0.508 vs 0.624) further supports the formulation's sustained drug release, ensuring steady plasma concentrations over time. These results underscore the enhanced pharmacokinetic profile of the FN4 formulation, achieved through its nanoparticle-based design.

The arabinoxylan-based nanoparticle formulation developed in this study demonstrates a substantial enhancement in solubility, leading to improved bioavailability and pharmacokinetic stability. The nanoparticles provide a sustained release profile, reducing plasma concentration fluctuations, thereby mitigating dose-related adverse effects such as akathisia, metabolic disturbances, and sedation. This novel approach offers a promising pharmacotherapeutic strategy by not only optimizing the systemic delivery of aripiprazole but also reducing the required dose and associated side

Table 7 Comparative Pharmacokinetic Parameters of APZ from Oral Suspension vs Optimized FN4 Formulation

Sr No.	Parameters	APZ suspension (Mean ± SD)	Optimized FN4 Formulation (Mean ± SD)	p-value
1	Lambda-z (h^{-1})	0.026 ± 0.003	0.053 ± 0.004	< 0.001
2	t1/2 (h)	8.772 ± 1.020	13.1924 ± 0.935	< 0.001
3	Tmax (h)	6.0 ± 0.5	12.0 ± 1.1	< 0.001
4	Cmax (ng/mL)	235 ± 1.56	742.333 ± 3.52	< 0.001
5	Tlag (h)	0 ± 0	0 ± 0	Not significant
6	Clast_obs/Cmax	0.624 ± 0.042	0.508± 0.056	< 0.001
7	AUC 0-t (ng/mL.h)	5789±1.60	10,362.749±1.66	< 0.001

effects. These improvements are expected to enhance patient compliance and long-term outcomes in managing psychiatric disorders, establishing arabinoxylan-based nanoparticles as a versatile platform for solubility-limited drugs.

Conclusion

This study presents a novel approach for enhancing the solubility and bioavailability of poorly soluble APZ by formulating AX-based nanoparticles. The unique aspect of this research lies in the use of arabinoxylan (AX), a natural polysaccharide derived from maize husk, as a drug carrier, offering a sustainable, biocompatible, and cost-effective alternative to synthetic polymers commonly used in nanoparticle formulations. The study demonstrates, for the first time, the successful encapsulation of APZ in AX-based nanoparticles, which was confirmed through FTIR analysis, indicating a strong interaction between APZ and AX. The nanoparticles exhibited enhanced dissolution rates of APZ in both simulated gastric and intestinal fluids (SGF and SIF), highlighting the potential for improving the solubility of this poorly water-soluble drug. Moreover, the in vitro characterization revealed that APZ was incorporated into the nanoparticles in an amorphous state, which is known to further enhance drug solubility. The small particle size and unique nanoscale structure of the formulated nanoparticles contributed to improved drug bioavailability. This innovative strategy, utilizing AX as a natural excipient for poorly soluble drugs, represents a significant advancement in drug delivery systems, providing a promising solution to overcome solubility challenges and improve the oral bioavailability of hydrophobic drugs like APZ.

Data Sharing Statement

The authors confirm that the data supporting the findings of this study are available within the article.

Ethics Statements

This research received ethics approval from the Ethics Committee of the Capital University of Science and Technology, Islamabad (Approval Ref# PREC/05/19).

Author Contributions

All authors have made substantial contributions to the work, including its conception, study design, execution, data acquisition, analysis, and interpretation. They all participated in drafting, revising, or critically reviewing the manuscript. Furthermore, all authors have approved the final version of the article, agreed on the journal for submission, and take full responsibility for all aspects of the work.

Funding

No funding for the research.

Disclosure

The authors declare no conflicts of interest in this work.

References

1. Shahzad Y, Maqbool M, Hussain T. et al. Natural and semisynthetic polymers blended orodispersible films of citalopram. *Natural Prod Res*. 2020;34(1):16–25. doi:10.1080/14786419.2018.1552698
2. Kim H, Lee JH, Kim JE, et al. Micro-/nano-sized delivery systems of ginsenosides for improved systemic bioavailability. *J Ginseng Res*. 2018;42 (3):361–369. doi:10.1016/j.jgr.2017.12.003
3. Jabeen N, Atif M. Polysaccharides based biopolymers for biomedical applications: a review. *Polym Adv Technol*. 2024;35(1):e6203. doi:10.1002/pat.6203
4. Kumar A, De A, Mozumdar S. Synthesis of acrylate guar-gum for delivery of bio-active molecules. *Bull. Mater. Sci.* 2015;38(4):1025–1032. doi:10.1007/s12034-015-0930-z
5. Zeidan TA, Trotta JT, Chiarella RA, et al. Polymorphism of dehydro-aripiprazole, the active metabolite of the antipsychotic drug aripiprazole (Abilify). *Cryst. Growth Des.* 2013;13(5):2036–2046.
6. Jin Z, Han Y, Zhang D, et al. Application of intranasal administration in the delivery of antidepressant active ingredients. *Pharmaceutics*. 2022;14 (10):2070. [2022, s Note: MDPI stays neutral with regard to jurisdictional claims in published]. doi:10.3390/pharmaceutics14102070
7. Begines B, Ortiz T, Pérez-Aranda M, et al. Polymeric nanoparticles for drug delivery: recent developments and future prospects. *Nanomaterials*. 2020;10(7):1403. doi:10.3390/nano10071403
8. Zingale E, Bonaccorso A, Carbone C, et al. Drug nanocrystals: focus on brain delivery from therapeutic to diagnostic applications. *Pharmaceutics*. 2022;14(4):691. doi:10.3390/pharmaceutics14040691
9. Valério R, Crespo JG, Galinha CF, et al. Effect of ultrafiltration operating conditions for separation of ferulic acid from arabinoxylans in corn fibre alkaline extract. *Sustainability*. 2021;13(9):4682. doi:10.3390/su13094682
10. de Mattos NR, Colodette JL, de Oliveira CR. Alkaline extraction and carboxymethylation of xylans from corn fiber. *Cellulose*. 2019;26 (3):2177–2189. doi:10.1007/s10570-018-02236-5
11. Patel MK, Tanna B, Gupta H, et al. Physicochemical, scavenging and anti-proliferative analyses of polysaccharides extracted from psyllium (Plantago ovata Forssk) husk and seeds. *Int J Biol Macromol*. 2019;133:190–201. doi:10.1016/j.ijbiomac.2019.04.062
12. Hegde RP, Rheingold JL, Welch S, et al. Studies of powder flow using a recording powder flowmeter and measurement of the dynamic angle ofrepose. *J Pharmaceut Sci*. 1985;74(1):11–15. doi:10.1002/jps.2600740104
13. Hamdani A, Rather SA, Shah A, et al. Physical properties of barley and oats cultivars grown in high altitude Himalayan regions of India. *Journal of Food Measurement & Characterization*. 2014;8(4):296–304. doi:10.1007/s11694-014-9188-1
14. Shah RB, Tawakkul MA, Khan MA. Comparative evaluation of flow for pharmaceutical powders and granules. *AAPS Pharm Sci Tech*. 2008;9 (1):250–258. doi:10.1208/s12249-008-9046-8
15. Kumar V, Taylor MK, Mehrotra A, et al. Real-time particle size analysis using focused beam reflectance measurement as a process analytical technology tool for a continuous granulation–drying–milling process. *AAPS Pharm Sci Tech*. 2013;14(2):523–530. doi:10.1208/s12249-013-9934-4
16. Calvo P, Remuñan-López C, Vila-Jato JL, et al. Chitosan and chitosan/ethylene oxide-propylene oxide block copolymer nanoparticles as novel carriers for proteins and vaccines. *Pharm Res*. 1997;14(10):1431–1436. doi:10.1023/A:1012128907225
17. Avadi MR, Sadeghi AMM, Mohammadpour N, et al. Preparation and characterization of insulin nanoparticles using chitosan and Arabic gum with ionic gelation method. *Nanomed Nanotechnol Biol Med*. 2010;6(1):58–63. doi:10.1016/j.nano.2009.04.007
18. Piazzini V, Landucci E, Urru M, et al. Enhanced dissolution, permeation and oral bioavailability of aripiprazole mixed micelles: in vitro and in vivo evaluation. *Int J Pharm*. 2020;583:119361. doi:10.1016/j.ijpharm.2020.119361
19. Shen J, Burgess DJ. In vitro dissolution testing strategies for nanoparticulate drug delivery systems: recent developments and challenges. *Drug Delivery Transl Res*. 2013;3(5):409–415. doi:10.1007/s13346-013-0129-z
20. Rwei S-P, Chuang -Y-Y, Way T-F, et al. Preparation of thermo-and pH-responsive star copolymers via ATRP and its use in drug release application. *Colloid. Polym. Sci.* 2015;293(2):493–503. doi:10.1007/s00396-014-3436-0
21. England CG, Miller MC, Kuttan A, et al. Release kinetics of paclitaxel and cisplatin from two and three layered gold nanoparticles. *Eur. J. Pharm. Biopharm.* 2015;92:120–129. doi:10.1016/j.ejpb.2015.02.017
22. Romero-Pérez A, García-García E, Zavaleta-Mancera A, et al. Designing and evaluation of sodium selenite nanoparticles in vitro to improve selenium absorption in ruminants. *Vet Res Commun*. 2010;34(1):71–79. doi:10.1007/s11259-009-9335-z
23. Barhoum A, García-Betancourt ML, Rahier H, Van Assche G. *Physicochemical Characterization of Nanomaterials: Polymorph, Composition, Wettability, and Thermal Stability, in Emerging Applications of Nanoparticles and Architecture Nanostructures*. Elsevier; 2018;255–278.
24. Hajizadeh-Oghaz M, Razavi RS, Barekat M, et al. Synthesis and characterization of Y 2 O 3 nanoparticles by sol–gel process for transparent ceramics applications. *J Sol Gel Sci Techn*. 2016;78(3):682–691. doi:10.1007/s10971-016-3986-3
25. Devangan P, Saini A, Patel D, Kolhe U. Solubility enhancement of aripiprazole via mesoporous silica: preparation, characterization, in vitro drug release, and solubility determination. *J Pharm Innovation*. 2023;18:1–12.
26. Shoueir KR, Atta AM, Sarhan AA, et al. Synthesis of monodisperse core shell PVA@P(AMPS- co -NIPAm) nanogels structured for pre-concentration of Fe(III) ions. *Environ. Technol.* 2017;38(8):967–978. doi:10.1080/09593330.2016.1215351
27. Sonavane G, Tomoda K, Sano A, et al. In vitro permeation of gold nanoparticles through rat skin and rat intestine: effect of particle size. *Colloids Surf. B*. 2008;65(1):1–10. doi:10.1016/j.colsurfb.2008.02.013
28. Pillai O, Panchagnula R. Transdermal delivery of insulin from poloxamer gel: ex vivo and in vivo skin permeation studies in rat using iontophoresis and chemical enhancers. *J Control Release*. 2003;89(1):127–140. doi:10.1016/S0168-3659(03)00094-4

29. Kunanusorn P, Panthong A, Pittayanurak P, et al. Acute and subchronic oral toxicity studies of Nelumbo nucifera stamens extract in rats. *J Ethnopharmacol*. 2011;134(3):789–795. doi:10.1016/j.jep.2011.01.037
30. Prabu P, Panchapakesan S, Raj CD. Acute and sub-acute oral toxicity assessment of the hydroalcoholic extract of Withania somnifera roots in Wistar rats. *Phytother Res*. 2013;27(8):1169–1178. doi:10.1002/ptr.4854
31. Alves JSF, Silva AMDS, da Silva RM, et al. In Vivo antidepressant effect of Passiflora edulis f. flavicarpa into cationic nanoparticles: improving bioactivity and safety. *Pharmaceutics*. 2020;12(4):383. doi:10.3390/pharmaceutics12040383
32. Yao W, Cheng J, Kandhare AD, et al. Toxicological evaluation of a flavonoid, chrysin: morphological, behavioral, biochemical and histopathological assessments in rats. *Drug Chem. Toxicol.* 2021;44(6):601–612. doi:10.1080/01480545.2019.1687510
33. Suman S, Gautam S. Pyrolysis of coconut husk biomass: analysis of its biochar properties. *Energy Sources Part A*. 2017;39(8):761–767. doi:10.1080/15567036.2016.1263252
34. Kedia K, Wairkar S. Improved micromeritics, packing properties and compressibility of high dose drug, Cycloserine, by spherical crystallization. *Powder Technol*. 2019;344:665–672. doi:10.1016/j.powtec.2018.12.068
35. Gooneh-Farahani S, Naghib SM, Naimi-Jamal MR. A novel and inexpensive method based on modified ionic gelation for pH-responsive controlled drug release of homogeneously distributed chitosan nanoparticles with a high encapsulation efficiency. *Fibers Polym*. 2020;21(9):1917–1926. doi:10.1007/s12221-020-1095-y
36. Zheng W, Jain A, Papoutsakis D, et al. Selection of oral bioavailability enhancing formulations during drug discovery. *Drug Dev. Ind. Pharm.* 2012;38(2):235–247. doi:10.3109/03639045.2011.602406
37. Sahu BP, Das MK. Nanosuspension for enhancement of oral bioavailability of felodipine. *Appl. Nanosci.* 2014;4(2):189–197. doi:10.1007/s13204-012-0188-3
38. Chavhan S, Joshi G, Petkar K, et al. Enhanced bioavailability and hypolipidemic activity of Simvastatin formulations by particle size engineering: physicochemical aspects and in vivo investigations. *Biochem. Eng. J.* 2013;79:221–229. doi:10.1016/j.bej.2013.08.007
39. Ding Z, Wang L, Xing Y, et al. Enhanced oral bioavailability of celecoxib nanocrystalline solid dispersion based on wet media milling technique: formulation, optimization and in vitro/in vivo evaluation. *Pharmaceutics*. 2019;11(7):328. doi:10.3390/pharmaceutics11070328
40. Malik NS, Ahmad M, Minhas MU, Murtaza G, Khalid Q. Polysaccharide hydrogels for controlled release of Acyclovir: development, characterization and in vitro evaluation studies. *Polym Bull*. 2017;74(10):4311–4328. doi:10.1007/s00289-017-1952-z
41. Khalid I, Ahmad M, Minhas MU, Barkat K. Synthesis and evaluation of chondroitin sulfate based hydrogels of loxoprofen with adjustable properties as controlled release carriers. *Carbohydr. Polym.* 2018;181:1169–1179. doi:10.1016/j.carbpol.2017.10.092
42. Jiang Y, Bai X, Lang S, et al. Optimization of ultrasonic-microwave assisted alkali extraction of arabinoxylan from the corn bran using response surface methodology. *Int J Biol Macromol*. 2019;128:452–458. doi:10.1016/j.ijbiomac.2019.01.138
43. Afrooz H, Mohamed EM, Barakh Ali SF, et al. Salt engineering of aripiprazole with polycarboxylic acids to improve physicochemical properties. *AAPS Pharm Sci Tech*. 2021;22(1):1–10. doi:10.1208/s12249-020-01875-x
44. Sawant K, Pandey A, Patel S. Aripiprazole loaded poly (caprolactone) nanoparticles: optimization and in vivo pharmacokinetics. *Mater Sci Eng C*. 2016;66:230–243. doi:10.1016/j.msec.2016.04.089
45. Hao S, Wang Y, Wang B, et al. Formulation of porous poly (lactic-co-glycolic acid) microparticles by electrospray deposition method for controlled drug release. *Mater Sci Eng C*. 2014;39:113–119. doi:10.1016/j.msec.2014.02.014
46. Amidon GE, Secreast PJ, Mudie D. Particle, powder, and compact characterization, in Developing solid oral dosage forms. *Elsevier*. 2009;163–186.
47. Zhou Y, Wang C, Liu W, et al. Fast in vitro release and in vivo absorption of an anti-schizophrenic drug paliperidone from Its Soluplus®/TPGS mixed micelles. *Pharmaceutics*. 2022;14(5):889. doi:10.3390/pharmaceutics14050889
48. Konno H, Handa T, Alonzo DE, et al. Effect of polymer type on the dissolution profile of amorphous solid dispersions containing felodipine. *Eur. J. Pharm. Biopharm.* 2008;70(2):493–499. doi:10.1016/j.ejpb.2008.05.023
49. Güncüm E, Işıklan N, Anlaş C, et al. Development and characterization of polymeric-based nanoparticles for sustained release of amoxicillin–an antimicrobial drug. *Artif. Cells Nanomed. Biotechnol.* 2018;46(sup2):964–973. doi:10.1080/21691401.2018.1476371
50. Salazar-Cruz BA, Chávez-Cinco MY, Morales-Cepeda AB, et al. Evaluation of thermal properties of composites prepared from pistachio shell particles treated chemically and polypropylene. *Molecules*. 2022;27(2):426. doi:10.3390/molecules27020426
51. Anirudhan TS, Anila MM, Franklin S. Synthesis characterization and biological evaluation of alginate nanoparticle for the targeted delivery of curcumin. *Mater Sci Eng C*. 2017;78:1125–1134.
52. Sadaquat H, Akhtar M, Nazir M, Ahmad R, Alvi Z, Akhtar N. Biodegradable and biocompatible polymeric nanoparticles for enhanced solubility and safe oral delivery of docetaxel: in vivo toxicity evaluation. *Int J Pharmaceutics*. 2021;598(120363):120363. doi:10.1016/j.ijpharm.2021.120363
53. Malik NS, Ahmad M, Alqahtani MS, et al. β-cyclodextrin chitosan-based hydrogels with tunable pH-responsive properties for controlled release of Acyclovir: design, characterization, safety, and pharmacokinetic evaluation. *Drug Delivery*. 2021;28(1):1093–1108. doi:10.1080/10717544.2021.1921074
54. Thai H, Thuy Nguyen C, Thi Thach L, et al. Characterization of chitosan/alginate/lovastatin nanoparticles and investigation of their toxic effects in vitro and in vivo. *Sci Rep*. 2020;10(1):1–15. doi:10.1038/s41598-020-57666-8
55. Bulgheroni A, Kinsner-Ovaskainen A, Hoffmann S, et al. Estimation of acute oral toxicity using the No Observed Adverse Effect Level (NOAEL) from the 28 day repeated dose toxicity studies in rats. *Regul Toxicol Pharmacol*. 2009;53(1):16–19. doi:10.1016/j.yrtph.2008.10.001
56. Akpanabiatu M, Igiri AO, Eyong EU, et al. Biochemical and histological effects of Eleophorbia drupifera leaf extract in Wistar albino rats. *Pharm Biol*. 2003;41(2):96–99. doi:10.1076/phbi.41.2.96.14242